Tension Leg Platform의 동적응답에 관한 연구

Dynamic Response of Tension Leg Platform

여 운 광*
Yeo, Woon Kwang
편 종 근**
Pyun, Chong Kun

요 지

Tension Leg Platform(TLP)이란 평형위치로부터 일정 범위내에서 움직임으로 인하여 외력의 효과를 완화시키는 compliant 구조물인 동시에, 기인장력을 받고 있는 연직 anchor cable이 있으므로 부력이 자중을 초과하게 되는 안정한 platform이다.

일반적으로 부체는 해상조건이 험할수록, 그리고 수심이 깊어질수록 동요가 심해지는데 TLP는 기인장 cable로 인하여 심해에서도 비교적 동요가 작아서 최근 대수심구조물의 총아로 각광받고 있다.

일찌기 Paulling 등이 TLP 거동의 예측을 위하여 수정된 Morison 방정식을 사용하는 선형동유체력합성방법을 발표하였다. 그러나 만일 TLP의 각 부재가 Morison 방정식의 가정이 성립할 수 없을 정도로 크다면 새로운 해석이 필요하다 하겠다. 일본의 Tanaka는 이런 경우에 McCamy-Fuchs 이론의 결과치를 이용하였으나, 완전한 해석이라기 보다는 일종의 간편법이라 하겠다.

본고에서는 큰 배수용적을 가진 연직부체가 있고, 이론적 해석의 결과를 검토해 볼 수 있는 수리모형 실험 결과가 있는 Deep Oil Technology (DOT) 회사의 TLP를 대상으로 하였다.

이 TLP는 부력을 전담하고 있는 연직축대칭 원통과 이들을 연결하고 있는 세부재로 이루어져 있어 축대칭부분에는 축대칭 Green 함수를 사용하여 동유체력을 구하고 세부재는 종래의 수정된 Morison 방정식의 항력항을 선형화하여 동유체력을 구하였다. 그리하여 부재의 각 미소부분에서 구한 힘들을 TLP의 중심에 원점을 둔 좌표계로 옮겨 동적응답을 구한 것이다.

본 해석에서 부재 상호간의 작용은 무시하였으며 단지 부재간의 거리효과만 고려하였다. 따라서 사용된 좌표계는 전체(Global) 좌표계, 지점(Local) 좌표계 및 파랑(Wave) 좌표계 등이었고 각 좌표계간의 변환식이 필요하였다.

전체적인 해석정도는 선형이론이므로 케이블의 강성도 역시 선형적으로 구하였으며, 앞서 언급했다시피 Morison 방정식의 비선형항인 항력항은 Fourier 해석으로 선형화 하였다. 이러한 Fourier 해석은 잘 알려져 있는 Lorentz 원리와 같다고 볼 수 있다. 세부재의 경우 접선력은 무시하였고 수입자의 운동에 의한 부재에 대한 수직력만 고려하였다. 여기서 파랑좌표계에서 지점좌표계로의 좌표

* 정회원·명지대학교 공과대학 전임강사, 토목공학과
** 정회원·명지대학교 공과대학 부교수, 토목공학과

변환이 주의를 요하고 있다.

이제 이렇게 구한 각 힘들을 전체좌표 계에서 6개의 자유도별로 운동방정식에 대입하면 각 자유도별 동적응답이 구하여지는 것이다.

DOT TLP의 Surge mode에 대한 동적응답을 실험치와 비교하여 본 결과, 세부재에 대한 고려를 뺄 수 없음을 알 수 있었다. 이는 연직축대칭 부체의 크기가 그리 크지 않으므로 인한 것이며, TLP의 원형의 경우에는 보다 더 관성력이 지배적일 것으로 사료된다.

Abstract

The tension leg platform (TLP) is a kind of compliant structures, and is also a type of moored stable platform with a buoyancy exceeding the weight because of having tensioned vertical anchor cables.

In this paper, among the various kinds of tension leg structures, Deep Oil Technology (DOT) TLP was analyzed because it has large-displacement portions of the immersed surface such as vertical corner pontoons and small-diameter elongated members such as cross-bracing. It also has results of hydraulic model tests, comparable with theorectical analysis. Because of the vertical axes of symmetry in the three vertical buoyant legs and because there are no larger horizontal buoyant members between these three vertical members, it was decided to develop a numerical algorithm which would predict the dynamic response of the DOT TLP using the previously developed numerical algorithm Floating Vessel Response Simulation (FVRS) for vertically axisymmetric bodies of revolution.

In addition, a linearized hydroelastic Morison equation subroutine would be developed to account for the hydrodynamic pressure forces on the small member cross bracing.

Interaction between the large buoyant members or small member cross bracings is considered to be negligible and is not included in the analysis.

The dynamic response of the DOT TLP in the surge mode is compared with the results of the TLP algorithm for various combinations of diffraction and Morison forces and moments. The results which include the Morison equation are better than the results for diffraction only. This is because the vertically axisymmetric buoyant members are only marginally large enough to consider diffractions effects. The prototype TLP results are expected to be more inertially dominated.

1. Introduction

The tension leg platform is a kind of compliant structures, which, as its name implies, are designed to move within excursion amplitudes from an equilibrium position so that the effects of the environmental load are mitigated,[1,2] and is a type of moored stable platform with a buoyancy exceeding the weight because of having tensioned vertical anchor cables.

Generally speaking, floating vessels, such as drill ship and a semisubmersible drilling rig, experience more heave, pitch, and roll motions as sea conditions become rougher and water depths greater. However, the tension leg platform, which is held firmly in place by vertical anchor cables, results in less motion response to heave, pitch and roll even in deep water.

Paulling and Horton[3,4] developed a method of predicting the TLP motions, using a linearized hydrodynamic synthesis technique, i.e.

the modified Morison's equation[5], which was also used by Burke[6] in the analysis of motions of semisubmersible drilling vessels in waves. The details of Paulling's method was also presented in Ref. (7) and(8).

Yashima had an interest in the experimental and theorectical study of a TLP in deep water[9] and Rainey indicated the dynamic instability at critical wave frequencies and subharmonic oscillations in cross seas[10]. Rowe and Jackson also experimented Mathieu instabilities on TBP[11]. Ashford and Wood took numerical integration of the motions of a TBP, neglecting drag term of the Morison equation[12]. Tanaka[13] introduced diffraction force based on McCamy-Fuchs' theory[14], because, if vertical pontoons of a TLP have a relatively large diameter, diffraction effects must be taken into consideration.

In this paper, among the various kinds of tension leg structures, the DOT TLP shown in Fig. 1 was analyzed because it has large-displacement portions of the immersed surface such as vertical corner pontoons and small-diameter elongated members such as cross-bracing. It also has results of hydraulic model tests, comparable with theorectical analysis.

This one-third scale model consists of a triangular shaped deck with three vertically axisymmetric circular cylinders at each corner of the triangular shaped deck. Smaller diameter circular cylinders connect each of these three vertical buoyant legs. Because of the vertical axes of symmetry in the three vertical legs and because there are no larger horizontal buoyant members between these three vertical members, it was decided to develop a numerical algorithm which would predict the dynamic response of the DOT TLP using the previously developed numerical algorithm FVRS for vertically axisymmetric bodies of revolution[15,16,17]. In addition, a linearized hydroelastic Morison

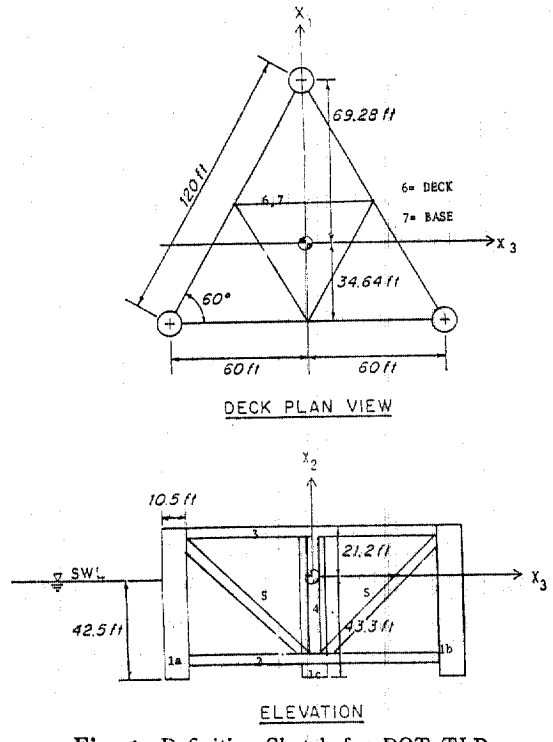

Fig. 1. Definition Sketch for DOT TLP

equation subroutine will be developed to account for the hydrodynamic pressure forces on the on the small member cross bracing {vide, Fig. 4}. This paper documents the theory and logic used to develop the TLP algorithm using the basic subroutines from the MARATHON FVRS plus the newly developed subroutines for the linearized hydroelastic Morison equation. A sample calculation and comparison with experimental results from the DOT TLP are also included.

2. Theoretical Modeling Assumptions

The TLP algorithm solves for the dynamic response of a TLP having vertically axisymmetric buoyant members and small member cross bracing. The dynamic response of the TLP in the global coordinate axes shown in Fig. 2 is obtained by solving for the hydrodynamic pressure forces on each member in

local member coordinates and then transforming these local forces back into the global coordinate axis by smiple coordinate transformations. Interaction between the large buoyant members or small member cross bracings is considered to be negligible and is not included in the analysis.

3. Coordinate System

3.1. Global Platform Coordinate Axis

The global coordinate axis for a platform having N vertically axisymmetric buoyant members is shown in Fig. 2. The X_1-X_3 plane lies parallel to the horizontal still water plane with the vertical X_2 axis positive up. Each buoyant member is rigidly connected to the platform deck. The origin of the global coordinate axis $\{X_1, X_2, X_3\}$ is located at the platform center of gravity {vide, Fig. 1}.

3.2. Local Body Coordinate Axes

A local body coordinate system for each of the N vertically axisymmetric buoyant body is aligned parallel to the global coordinate system with each of the axes origin located

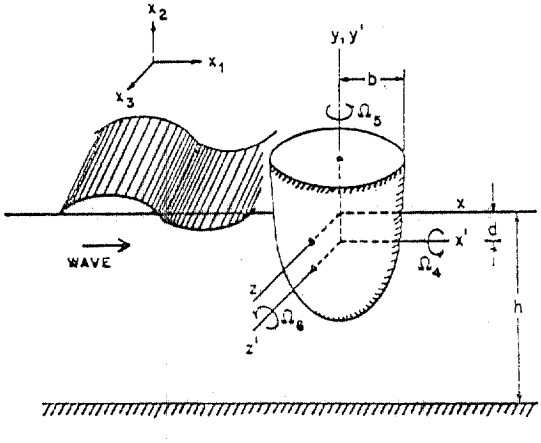

Fig. 2. Definition Sketch for Global, Local, and Wave Coordinate Axes for N Buoyant Diffraction Bodies

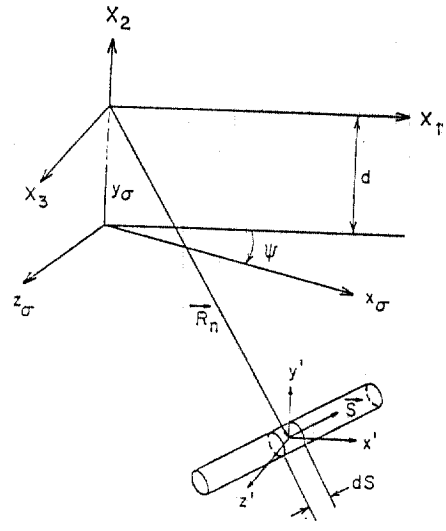

Fig. 3. Definition Sketch for Global, Local and Wave Coordinate Axes for N Hydroelastic Morison Members

at the center of gravity for each axisymmetric buoyant local body {vide, Fig. 2}. A local body coordinate system for each of the N' hydroelastic Morison members is shown in Fig. 3. A position vector $\vec{R}_n$ defines the distance from the global coordinate axes at the TLP center of gravity to the n^{th} local body coordinate axis at the local body center of gravity for both the vertically axisymmetric buoyant bodies and the hydroelastic Morison members according to

$$\vec{R}_n = X_{1n}\,\vec{e}_1 + X_{2n}\,\vec{e}_2 + X_{3n}\,\vec{e}_3 \qquad (1)$$

3.3. Wave Coordinate Axis

Monochromatic, long-crested, linear waves are assumed to be propagating without change of form at a constant angle of attack, ψ, shown in Fig. 3. Hydrodynamic interaction is neglected between either the large vertically axisymmetric buoyant diffraction bodies or the hydroelastic Morison member cross bracings. Consequently, neither the scattered wave field from the buoyant diffraction bodies nor the shielding effect from the hydroelastic Morison

member cross bracings are included in the determination of the local hydrodynamic pressure forces. This assumption appears to be experimentally justified by the DOT TLP data comparisons.

3.4. Local to Global Coordinate Transformations

The TLP is assumed to have six degrees of freedom in dynamic response to the waves; viz., three translational modes $\{X_1, X_2, X_3\}$ and three rotational modes $\{\Omega_4, \Omega_5, \Omega_6\}$ {vide, Fig. 2}. The n^{th} local body translational displacements may be expressed in terms of the global coordinates according to

$$\vec{X}_n=\vec{X}-\vec{R}_n\times\vec{\Omega} =\{x', y', z'\} \quad (2)$$

and the n^{th} local rotational displacements by

$$\vec{\omega}_n=\vec{\Omega} \quad (3)$$

The velocity and acceleration of the n^{th} local body are obtained from the temporal derivatives of Eqs. (2) and (3), respectively, i.e.,

$$\vec{u}_n=\dot{\vec{X}}-\vec{R}_n\times\dot{\vec{\Omega}} \quad (4a)$$

$$\dot{\vec{\omega}}_n=\dot{\vec{\Omega}} \quad (4b)$$

$$\vec{a}_n=\ddot{\vec{X}}-\vec{R}_n\times\ddot{\vec{\Omega}} \quad (5a)$$

$$\ddot{\vec{\omega}}_n=\ddot{\vec{\Omega}} \quad (5b)$$

4. Forces and Moments

4.1. Hydrodynamic Pressure Forces on n^{th} Local Body

The hydrodynamic pressure forces on the n^{th} local body due to long crested, linear waves propagating at an angle, ψ, to the global coordinate axes are assumed to be linearly decomposed into three separate component: viz., 1) hydrostatic restoring force; 2) wave-induced exciting force on a fixed body; and 3) wave-induced reacting force on a body oscillating in otherwise still water (wavemaker force). In an earlier MARATHON report for the FVRS, it was shown that for bodies having vertical axes of symmetry, only three modes of rigid body motion are possible {viz., 1) surge; 2) heave; and 3) pitch}. Consequently, only these three exciting and reacting forces will be computed for each large buoyant diffraction body. The procedure to be used to compute these forces will be to compute the hydrodynamic pressure force for each vertical member in the wave coordinate system and to then transform these forces back to the global coordinate system to solve for the dynamic response of the TLP.

For the wave coordinate system shown in Fig. 2, the following exciting forces will be computed

F_1^w=horizontal surge exciting wave force in wave direction (6a)

F_2^w=vertical heave exciting wave force (6b)

M_6^w=overturning pitching moment about the axis perpendicular to wave direction (6c)

The wave-induced exciting forces will then be transformed back to the global coordinate axis according to

$$\vec{F}_n^e=\{F_1^w\cos\psi,\ F_2^w, F_1^w\sin\psi\}_n \quad (7a)$$

$$\vec{M}_n^e=\{M_6^w\cos(\psi+\pi/2), 0, M_6^w\sin(\psi+\pi/2)\}_n \quad (7b)$$

The force and moment components are defined in APPENDIX A. The wave will be referenced to the global coordinate axis by

$$\tau_n=\vec{R}_n\cdot\vec{k}/\sigma \quad (8)$$

where

$$\vec{k}=\{k\cos\psi, 0, k\sin\psi\} \quad (9)$$

provided that

$$\sigma^2=(2\pi/T)^2=gk\tanh kh \quad (10)$$

The wave-induced exciting forces and moments computed by the MARATHON FVRS algorithm are complex-valued coefficients expressed by magnitude and phase[15,16,17].

The complex-valued, wave-induced hydro-

dynamic reacting forces are linearly decomposed into an added mass and a radiation damping component. The added mass, $\vec{F}_n^I$, and radiation damping, $\vec{F}_n^D$, components are given by

$$\vec{F}_n^1=\sum_{i=1}^{3}\sum_{j=1}^{6} {}_nM_{ij}\, a_{nj}\, \vec{e}_j \tag{11a}$$

$$\vec{F}_n^D=\sum_{i=1}^{3}\sum_{j=1}^{6} {}_n N_{ij}\, u_{nj}\, \vec{e}_j \tag{11b}$$

where

$$u_{nj}=\delta_{j1}\, x_n^1+\delta_{j2}\, y_n^1+\delta_{j3}\, z_n^1+\delta_{j4}\omega_{n4} +\delta_{j5}\,\omega_{n5}+\delta_{j6}\,\omega_{n6} \tag{11c}$$

$$a_{nj}=\dot{u}_{nj} \tag{11d}$$

and ${}_nM_{ij}$ and ${}_nN_{ij}$ are the complex-valued added mass and radiation damping components, respectively, defined in APPENDIX B.

4.2. Body Force/Moment

The inertial body force, $\vec{F}_n^B$, for the n^{th} local body in the local body coordinate is given by

$$\vec{F}_n^G=\sum_{i=1}^{6}\sum_{j=1}^{6} m_{nij}\, a_{nj}\, \vec{e}_j \tag{12}$$

in which

$$m_{nij}=\sum_{l=1}^{3}\delta_{li}\,\delta_{lj}\, m_n+\sum_{l=4}^{6}\{\delta_{lj}\delta_{li}-|e_{lij}|\}\, I_{nij} \tag{13}$$

where $m_n=n^{th}$ local body mass; e_{lij}=permutation symbol; and the moment of inertia is defined by

$${}_{nij}=\sum_{l=4}^{6}\delta_{li}\,\delta_{lj}\iint x_{ni}\, x_{nj}\, dA \tag{14}$$

4.3. Hydrostatic Restoring Force/Moment

The hydrostatic restoring force/moment are given by

$$\vec{F}_n^H=\sum_{i=1}^{3} k_{ni}\,\vec{x}_{ni} \tag{15a}$$

$$\vec{M}_n^H=\sum_{i=4}^{6}\sum_{j=1}^{6} k_{nj}\,\vec{\Omega}_{nj} \tag{15b}$$

4.4. Mooring Restoring Force/Moment

The restoring force exerted by the tether bundles on the TLP may be expressed by

$$\vec{F}_n^M=\sum_{j=1}^{3} k_{nj}\,\vec{x}_{nj} \tag{16a}$$

$$\vec{M}_n^M=\sum_{j=4}^{6} k_{nj}\,\vec{\Omega}_{nj} \tag{16b}$$

4.5. Hydroelastic Morison Force/Moment

The small member cross bracings shown in Fig. 1 do not lie in the diffraction force regime as do the large vertically axisymmetric corner members. Forces on these small members must be computed by a linearized hydroelastic Morison equation. The coordinate system used for the small member hydroelastic Morison force is shown in Fig. 5.

By generalizing the one-dimensional form of the Morison equation, the three-dimensional form of the hydrodynamic force acting normally to the n^{th} hydroelastic Morison small member element is given by

$$\vec{F}_n^S=(C_m-1)\rho V(\dot{\vec{V}}_n-\ddot{\vec{x}}_n) +C_D\frac{\rho}{2}A\,|\vec{V}_n-\dot{\vec{x}}_n|\,(\vec{V}_n-\dot{\vec{x}}_n)+\rho V\dot{\vec{V}}_n \tag{17}$$

in which C_m, C_D=inertia and drag coefficients, respectively; $\dot{\vec{V}}_n, \vec{V}_n$=local water particle acceleration and velocity normal to the member at the center of the n^{th} small member element, respectively; $\ddot{\vec{x}}_n$, $\dot{\vec{x}}_n$=motion-induced member acceleration and velocity normal to the member at the center of the n^{th} small member element, respectively; ρ=fluid mass density; and V, A=volume and normal area projection of the n^{th} small member element, respectively.

If we use the approximate relation

$$|\vec{V}_n-\dot{\vec{X}}_n|\,(\vec{V}_n-\dot{\vec{X}}_n)\simeq|\vec{V}_n|\,\vec{V}_n-2|\vec{V}_n|\,\dot{\vec{X}}_n \tag{18}$$

according to the equation (7, 12) of the reference[1] then the equation (17) may be linearly decomposed into a wave-induced exciting force for a fixed body and a motion-induced reacting

force on a body oscillating in other-wise still water by

$$\vec{F}_n{}^s=\vec{F}_n{}^e-\vec{F}_n{}^R \tag{19a}$$

$$=C_m\rho V\dot{\vec{V}}_n+C_D\frac{\rho}{2}A|\vec{V}_n|\vec{V}_n$$

$$-(C_m-1)\rho V\ddot{\vec{X}}_n-2C_D\frac{\rho}{2}A|\vec{V}_n|\dot{\vec{X}}_n \tag{19b}$$

The quadratic drag force term in the exciting force proportional to $|\vec{V}_n|\vec{V}_n$ and the quadratic viscous damping term in the reacting force proportional to $|\vec{V}_n|\dot{\vec{X}}_n$ are linearized by Fourier analysis according to

$$|\vec{V}_n|\,V_{nj}=U_{nj}\exp(-i\omega t);\ j=1,2,3 \tag{20a}$$

$$|V_n|\frac{\dot{\vec{X}}_{nj}}{|\dot{\vec{X}}_{nj}|}=X_{nj}\exp(-i\omega t);\ j=1,2,3 \tag{20b}$$

in which the complex valued coefficients U_{nj} and X_{nj} are computed by Fourier analysis, and the suffix j stands for the j^{th} direction of the axis of the cartesian global coordinate. Note that only a unit velocity for the member is used to linearize the quadratic viscous damping term in Eq. (20b).

The water particle velocity vector, $\vec{V}_n$; normal to the member at the center of the n^{th} small member element, is estimated from linear wave theory kinematics by

$$\vec{V}_n=\begin{Bmatrix}V_{n1}\\V_{n2}\\V_{n3}\end{Bmatrix}=\begin{bmatrix}1-\theta_{11}{}^2, & -\theta_{11}\theta_{12}, & -\theta_{11}\theta_{13}\\ -\theta_{11}\theta_{12}, & 1-\theta_{12}{}^2, & -\theta_{12}\theta_{13}\\ -\theta_{11}\theta_{13}, & -\theta_{12}\theta_{13}, & 1-\theta_{13}{}^2\end{bmatrix}\begin{Bmatrix}U_{n0}\\V_{n0}\\W_{n0}\end{Bmatrix} \tag{21}$$

where θ_{11}, θ_{12} and θ_{13} are the directional cosines of unit vector along the axis of the small member element in the global coordinate where

$$U_{n0}=A\cos\psi\cos h\,k\delta\exp i\,\omega\varepsilon_n$$

$$V_{n0}=A\sin h\,k\delta\exp i\left(\omega\varepsilon_n-\frac{\pi}{2}\right)$$

$$W_{n0}=A\sin\psi\cos k\delta\exp i\,\omega\varepsilon_n$$

and where

$$A=\frac{Hgk}{2\omega}\ \mathrm{sech}kh$$

$$\delta=Y_n+d+h$$

The corresponding hydrodynamic pressure moment induced on the global structure by Eq. (18) on the n^{th} local member may be expressed as

$$M_n{}^S=\vec{R}_n\times\vec{F}_n{}^e-\vec{R}_n\times\{\vec{F}_n{}^I+\vec{F}_n{}^V\} \tag{22}$$

5. Equation of Motion for TLP

The preceding forces/moments on the N individual buoyant diffraction members plus the N' individual segments of the hydrostatic Morison member cross bracing are assembled to give the dynamic equations of motion for TLP in the global coordinates according to

$$\sum_{n=1}^{N}\{\vec{F}_n{}^I+\vec{F}_n{}^D+\vec{F}_n{}^H+\vec{F}_n{}^M\}+\sum_{n=1}^{N'}\{\vec{F}_n{}^I+\vec{F}_n{}^V\}$$

$$+\vec{F}^G=\sum_{n=1}^{N}\vec{F}_n{}^e+\sum_{n=1}^{N'}\vec{F}_n{}^e \tag{23a}$$

$$\sum_{n=1}^{N}\{\vec{M}_n{}^I+\vec{M}_n{}^D+\vec{M}_n{}^H+\vec{M}_n{}^M\}+\vec{M}^G$$

$$+\sum_{n=1}^{N}\vec{R}_n\times\{\vec{F}_n{}^I+\vec{F}_n{}^D+\vec{F}_n{}^H+\vec{F}_n{}^M\}$$

$$+\sum_{n=1}^{N'}\vec{R}_n\times\{\vec{F}_n{}^I+\vec{F}_n{}^V\}$$

$$=\sum_{n=1}^{N}\vec{M}_n{}^e+\sum_{n=1}^{N}\vec{R}_n\times\vec{F}_n{}^e+\sum_{n=1}^{N'}\vec{R}_n\times\vec{F}_n{}^e \tag{23b}$$

in which N=total number of large vertically axisymmetric buoyant members and N'=total number of small member elements.

6. Example Problem for DOT TLP and Conclusion

Experimental response data recorded for the

DOT TLP were compared with the TLP algorithm output. The 1 : 3 scale model DOT TLP shown in Fig. 1 dimensionless numerals stand for the number of members consists of three vertically axisymmetric buoyant caissons located at each apex of the triangular shaped deck structure; 3 each exterior and interior horizontal cross bracing members at base level and main deck level; 3 vertical small member columns; and 6 diagonal interior struts. Forces and moments on the three vertically axisymmetric buoyant caissons were computed by the Green's function diffraction method using the MARATHON FVRS algorithm; while the forces and moments on all of the remaining small members were computed by the linearized hydroelastic Morison equation method.

The discretization scheme used to compute the forces/moments on the DOT TLP is shown in Fig. 4. Each vertically axisymmetric buoyant pontoon was discretized into eight nodal points beginning at the submerged center line of the vertically axisymmetric member (0, −42.6) and ending at the still water level (5.25, 0). For identical vertically axisymmetric buoyant caissons, only the nodal points for one of the identical caissons must be input into the TLP algorithm. The algorithm automatically transforms each of the forces and moments for identical vertical axisymmetric caissons into the global C.G. using the global coordinates of each local body C.G. Each of the three horizontal exterior cross bracing members were discretized into ten equal segments for analysis by the linearized hydroelastic Morison equation (vide, Fig. 4). Each of the three vertical small member columns and each of the six diagonal small member interior struts were discretized into five equal segments for analysis by the linearized hydroelastic Morison equation (vide, Fig. 4).

A flow chart of the TLP algorithm and the

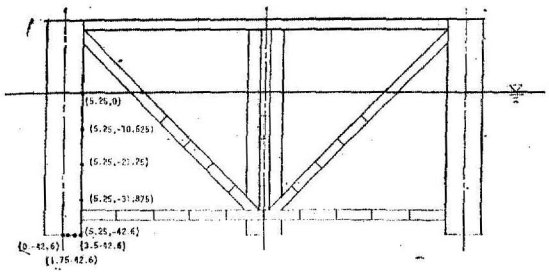

Fig. 4.

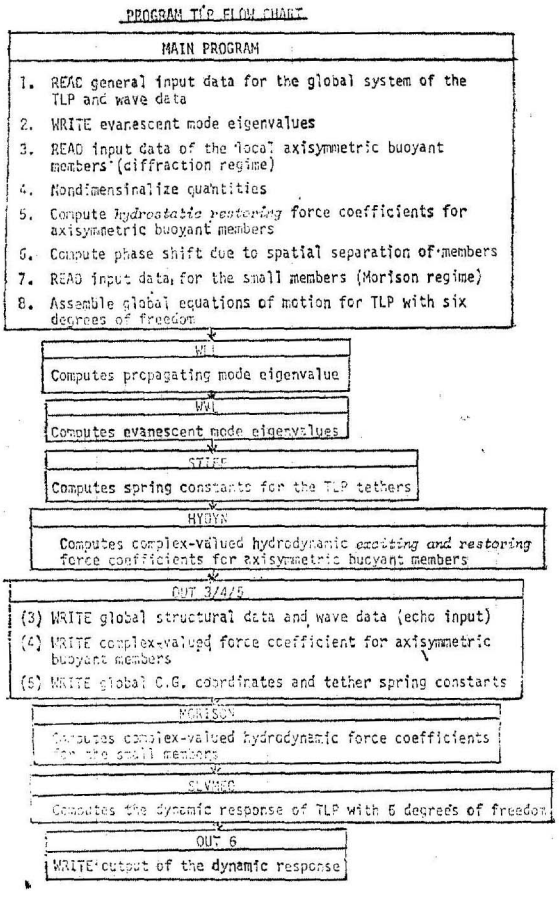

Fig. 5.

primary SUBROUTINES HYDYN, MORISON and SLMEQ are provided (vide, Fig. 5).

The dynamic response of the DOT TLP in the surge mode is compared in Fig. 6 with the results of the TLP algorithm for various com-

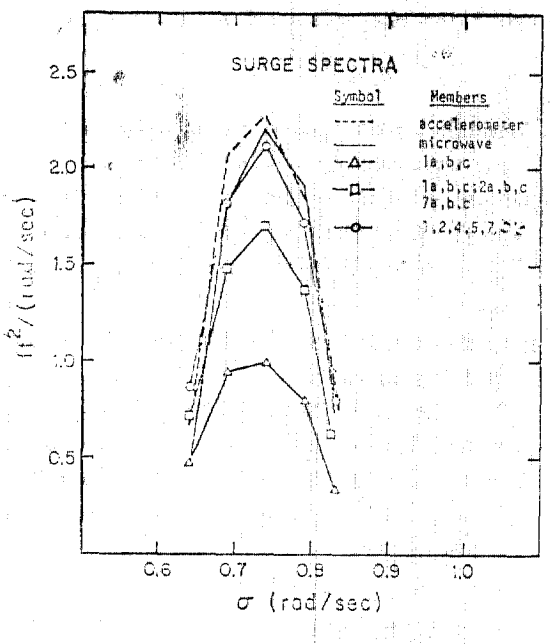

Fig. 6. Surge Spectrum for DOT TLP

binations of diffraction and Morison forces and moments. The results which include the Morison equation are better than the results for diffraction only. This is because the vertically axisymmetric buoyant members are only marginally large enough to consider diffraction effects. The prototype TLP results are expected to be more inertially dominated. The five frequencies used to compute the surge mode RAO in Fig. 6 were taken from the DOT WAVE-2 spectrum for 0° angle of attack in the global coordinate axis.

감사의 말씀

이 논문은 아산사회복지사업재단의 1982년도 연구비 지원에 의하여 연구되었으므로 이에 감사를 드린다.

References

1. Zienkiewicz, O.C., Lewis, R.W. and Stagg, K.G., *Numerical Methods in Offshore Engineering*, Wiley, New York, 1978, pp. 10~12.
2. Sarpkaya, T. and Isaacson, M., *Mechanics of Wave Forces on Offshore Structures*, Van Nostrand, New York, 1981, pp. 4~5.
3. Paulling, J.R. and Horton, E.E., "Analysis of the Tension Leg Platform", *SPE Journal*, Sep., 1971, pp. 285~294.
4. Horton, E.E., McCommon, L.B., Murtha, J.P. and Paulling, J.R., "Optimization of Stable Platform Characteristics", *Proc. OTC*, Paper No. OTC 1553, 1972, pp. 1~417, 1~428.
5. Sarpkaya, T., "Morison's Equation and the Wave Forces on Offshore Structures", *CR 82.008*, Naval Cival Engineering Laboratory, Port Hueneme, Calif. 1981, pp. 31~33.
6. Burke, B.C., "The Analysis of Motions of Semisubmersible Drilling Vessels in Waves", *SPE Journal*, 1970, pp. 311~320.
7. Paulling, J.R., "Wave Induced Forces and Motions of Tubular Structures", *Proceedings, Eighth Symposium on Naval Hydrodynamics*, ACR-179, Office of Naval Rerearch, 1970, pp. 1083~1110.
8. Paulling, J.R., "Paper 25. Elastic Response of Stable Platform Structures to Wave Loading" Proc. Intl. Symp On Dynamics of Marine Vehicles and Structures in Waves", *Inst. of Mech. Engr.*, London, 1974, pp. 248~257.
9. Yashima, N., "The Experimental and Theoretical Study of a Tension Leg Platform in Deep Water", *Proc. OTC* Paper No. OTC 2690, 1976, pp. 849~856.
10. Rainey, R.C.T., "The Dynamics of Tethered Platforms", *The Roy. Inst. of Nav. Arch.*, 1977, pp. 59~80.
11. Rowe, S.J. and Jackson, G.E., "An Experimental Investigation of Mathieu Instabilities on Tethered Buoyant Platform Models", *OTR-8008*, National Maritime Institute, Jan., 1980, 32p.
12. Ashford, R.A. and Wood, W.L., "Numerical Integration of the Motions of a Tethered Buoyant Platform", *Int. Journ. for Nume. Meth. in Eng.*, Vol. 13, 1978, pp. 165~180.
13. Tanaka, Y., "Motions and Mooring Characteristics of Tension Leg Buoyant Bodies", *Conf. of Coastal Eng. (27th) in Japan*, 1980, pp. 280~

284.

14. MacCamy, R.C. and Fuchs, R.A., "Wave Forces on Piles; A Diffraction Theory", *Tech. Memo. No. 69*, U.S. Army corps of Engineers, Beach Erosion Board, 1954.
15. Hudspeth, R.T., Nakamura, T. and Leonard, J.W. "Floating Vessel Response Simulation (FVRS) by an Axisymmetric Green's Function", *Marathon Oil Company Report*, june, 1980, 46p.
16. Hudspeth, R.T., Nakamura, T. and Leonard, J.W., "User's Manual Floating Vessel Response Simulator FVRS", *Marathon Oil Co. Report*, June, 1980, 96p.
17. Pyun, C.K., "Dynamic Response of Vertical Axisymmetric Floating Bodies", *Proc. of the KSCE*, Vol. 4, No. 1, March, 1984, pp. 113~124.

Appendix A : Wave-Induced Exciting Force/Moment

The wave-induced hydropynamic exciting force/moment on each buoyant vertically axisymmetric body is computed by the axisymmetric Green's function method described in Refs. 15) and 17) Each force/moment must be transformed from the local body coordinate system to the global TLP coordinate system.

First, the wave is referenced to the global coordinate system according to the spatial phase angle

$$\tau_n=\vec{k}\cdot\vec{R}_n/\sigma \tag{A-1}$$

The translational force components in Eq. (7a) for the n^{th} vertically axisymmetric buoyant body in the local coordinate system are given by

$$F_1^w|C_1|{}_n\rho g b_n^3(k_0h)(H/2b_n)\cos\{\sigma(t-\tau_n)_n-\varepsilon_1\} \tag{A-2}$$

$$F_2^w|C_2|{}_n\rho g b_n^3(k_0h)(H/2b_n)\sin\{\sigma(t-\tau_n)_n-\varepsilon_2\} \tag{A-3}$$

in which C_i=complex-valued exciting force coefficient for the i^{th} mode computed by the axisymmetric Green's function method. The exciting moment component in Eq. (7b) is given by

$$M_g^w|C_6|{}_n\rho g b_n^4(k_0h)(H/2b_n)\cos\{\sigma(t-\tau_n)_n-\varepsilon_6\} \tag{A-4}$$

in which C_6=complex-valued exciting moment coefficient for pitch computed by the axisymmetric Green's function method.

Appendix B : Wave-Induced Reacting Force/Moment

The wave-induced hydrodynamic reacting force/moment on each vertically axisymmetric body is computed by the axisymmetric Green's function method described in Refs 15) and 17) Each force/moment is transformed from the local body coordinate system to the global TLP coordinate system as described in Appendix A.

The dimensional added mass, M_{ij}, and radiation damping coeffcients, N_{ij}, for the nth body are defined from the dimensionless complex-valued coefficients (C_{ij}) computed by the MARATHON FVRS algorithm according to

$${}_nM_{11}={}_nM_{33}=(\rho b_n^3)\mathrm{Real}\{C_{11}\} \tag{B-1}$$

$${}_nM_{22}=(\rho b_n^3)\mathrm{Real}\{C_{22}\} \tag{B-2}$$

$${}_nM_{16}={}_nM_{61}=(\rho b_n^4)\mathrm{Real}\{C_{16}\} \tag{B-3}$$

$${}_nM_{15}={}_nM_{51}={}_nM_{14}={}_nM_{41}={}_nM_{12}={}_nM_{21}={}_nM_{13}={}_nM_{31}=0 \tag{B-4}$$

$${}_nM_{23}={}_nM_{32}={}_nM_{24}={}_nM_{42}={}_nM_{25}={}_nM_{52}={}_nM_{26}={}_nM_{62}=0 \tag{B-5}$$

$${}_nM_{34}={}_nM_{43}=(\rho b_n^4)\mathrm{Real}\{C_{34}\} \tag{B-6}$$

$${}_nM_{44}={}_nM_{66}=(\rho b_n^5)\mathrm{Real}\{C_{66}\} \tag{B-7}$$

$${}_nM_{55}=0 \tag{B-8}$$

Appendix C : Tether Bundle Stiffness, k_{nj}

The tether bundle stiffness, k_{nj}, given in Eqs. (16) are determined from the initial tether tensions and the direction cosines, θ_j, for the static offset from a vertical equilibrium position. Assuming that each individual tether bundle is connected to the nth buoyant axisymmetric caisson at its center of gravity, C.G., the stiffness matrix is given by

$$K_{nj}=\sum_{i=1}^{3}\left\{\frac{T_0}{L}\delta_{ij}+\left(\frac{AE}{L}-\frac{T_0}{L}\right)\theta_i\theta_j\right\} \tag{C-1}$$

in which A=total cross-sectional area of the tether bundle; E=modulus of elasticity of tether material; L=total static length of tether bundle; and T_0=static tension of tether bundle. Note that there are no stiffness elements for the rotational degrees of freedom.

(接受 : 1984. 10. 8)